AISTech 2025 — Proceedings of the Iron & Steel Technology Conference
5–8 May 2025, Nashville, Tenn., USA
DOI: 10.33313/389/133

Multiphysics Model of Heat Transfer and Combustion in Continuous Casting Mold Powders

Lipsa Das[1], Adnan Akhtar[2], Brian G. Thomas[2]

[1]Department of Mechanical Engineering, Colorado School of Mines
1610 Illinois Street, Golden, Colorado, USA, 80401
Phone: 303-273-3309
Email: bgthomas@mines.edu
lipsadas@mines.edu

[2]ANSYS R&D
Austin, Texas, USA, 78746
Phone: 844-462-6797
Email: adnanakhtar1409@gmail.com

ABSTRACT

In continuous casting of steel, mold powder is added to the top surface to provide thermal insulation, lubrication, and to prevent liquid metal oxidation. Understanding powder melting behavior is key to maintaining a stable liquid slag pool thickness. A model of temperature distribution, combustion and gas reactions in the powder/slag layers has been developed. The powder/slag is modeled with a 1-D, fixed-grid, transient, advection-diffusion model, including phase changes, melting, powder densification, carbon burning, gas evolution, transport, and exhaust behaviors. The model is validated with measurements in a lab-scale sintering experiment, and with plant measurements in a commercial caster. The sintering during heating of mold powders decreases the pore fraction (fewer pore spaces), due to closer particle packing, neck formation and coalescence of powder particles. The powder densifies with time (and with distance down the layer), and melts to form liquid flux. During this period, the free carbon burns, producing a carbon depleted region in the middle region of the powder, and a carbon rich layer at the bottom of the sinter zone. The liquid flux layer builds with powder addition, heating, melting, and continuous feeding into the gap. This takes a long time, so steady state is unlikely to be reached in commercial operations. Intermittent powder addition leads to high temperature fluctuations at the powder top surface, especially if the time between additions is large.

Keywords: Heat Transfer, Powder Melting, Carbon Combustion, Gas Transport, Computational Model

INTRODUCTION

In continuous casting of steel, as shown in Figure 1 (a), mold powder is added to the top surface of the molten steel in the mold to provide thermal insulation, to prevent reoxidation, to absorb inclusions from the molten steel, to lubricate the gap between the solidifying steel shell and oscillating water-cooled copper mold and thereby to prevent friction, to control heat transfer across the gap, and to help in removal of impurities in the molten steel by absorbing inclusions such as alumina. For any reason, if any of the above functions cannot occur properly, this can lead to quality problems, such as mold powder entrapment (depending on fluid flow and surface tension, etc.), insufficient liquid flux feeding into the gap, thereby increasing friction, leading to various surface defects, and in severe cases, even breakouts.

While heat transfer across the interfacial gap is important to steel surface quality, vertical heat transfer through the top-surface mold powder is essential to provide stable melting, to prevent reoxidation and meniscus freezing, and to avoid contamination, such as carbon pickup from the sintered layer coming into contact with the molten steel. The melting rate should be controlled to provide sufficient liquid flux flow into the gap for proper lubrication, while not being excessive. It is important to maintain a stable liquid slag layer that is thick enough to completely cover the molten steel, in order to avoid contact of the carbon-rich sintered layer with the molten steel, and to provide continuous feeding into the interfacial gap. However, the liquid slag layer should not be allowed to become too thick, or it is easy to form defects due to mold slag entrainment from the shear flow across the top surface, and due to large, detrimental slag rims that form during the level fluctuations.

© 2025 by the Association for Iron & Steel Technology.

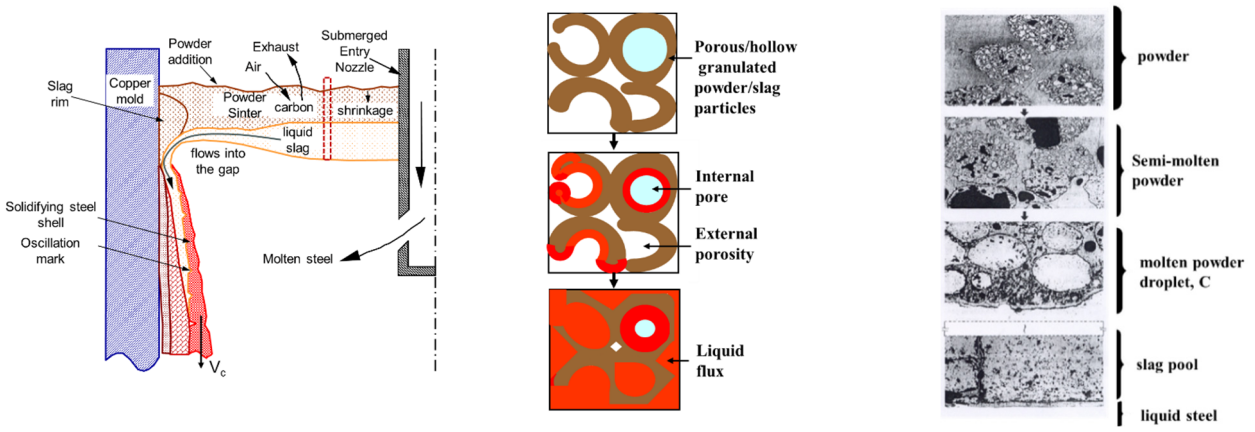

Figure 1: Continuous casting process in the mold with powder layers including (a) Schematic of phenomena with current model domain (red dotted rectangle).[1] (b) Schematic of porous/hollow granulated powder/slag particles sintering and gradually melting and (c) Micrographs of the powder sintering process[2].

The mold powder can be either granulated powder or ordinary fine powder. Figure 1 (b) and (c) show the transient sintering and melting process as powder particles move from top to bottom of the layer. In order to control the melting rate, both types of powder are mixed with a prescribed amount of carbon, either integrated into the powder, or as separate carbon particles, called "free carbon". The granulated powders investigated in this study are manufactured such that the powder is heated with air to make the contents explode, creating hollow shells of the various oxides that comprise the powder. The size of non-granulated powder/slag particles can range from 5-150μ, while that of the granulated powder/slag particles vary from 80-800 μ. The size of graphite particles is ~45 μ.[3]The top layer of the powder in the mold consists of the loose particles, as added from either an automated powder feeder or by pouring manually from a bag. These particles gradually undergo sintering and densification to produce a dense, C-enriched sinter layer towards the bottom and liquid slag. The sintered layer gradually accumulates carbon which has not burned away. The liquid slag gradually is drawn downward to form a molten slag/layer that floats above the molten steel. Towards the meniscus region, the liquid is consumed into the gap between the solidifying steel shell and the copper mold wall during the oscillation cycles. Liquid slag consumed in this way acts to lubricate the gap between shell and mold, prevent friction, and regulate heat transfer in the gap.

The carbon in the casting powder controls the melting rate and undergoes combustion through several chemical reactions leading to the formation of carbon dioxide and carbon monoxide. These reactions are controlled by both chemical kinetics and diffusion due to the transport of oxygen into the powder, and the transport of combustion products upwards and out of the powder top surface. In work by Schwerdtferger et al[5], it is reported that combustion is controlled by chemical reaction at low temperatures (300-400°C), and by mass transfer inside the powder and gas at high temperatures (600-800°C). A region of mixed control is described to be present between these temperatures. The top powder zone is too cold to enable the combustion reactions to occur. Oxygen diffusing down from the ambient reacts with carbon to form carbon dioxide, where the temperature is cooler in the upper powder. Some carbon dioxide diffuses further downwards, and at the higher temperatures near the powder bottom facilitates the formation of carbon monoxide. At intermediate distances, the carbon burns to form a mixture of CO and CO_2. As the gas percolates upwards and cools, CO further decomposes into CO_2.

Relatively little work has been done to model the complete phenomena involving mold powder described in the previous section. Some work has been done to study heat transfer in mold powders.[2, 6, 7,8.] However, the gas behavior was not included in these studies. Recently, Supradist et al [9] modeled the heat transfer and gas reactions in lab sintering experiments and matched several temperature, carbon, and gas distribution measurements. However, they did not apply the model to the continuous casting process. Several experiments[9,10,11,12] and models[13,14,15,16] in previous literature predict the thermal behavior in continuous casting mold powders. A coupled fluid flow and heat transfer study of the liquid flux layer was done by McDavid and Thomas[13] using a 3-D model with the finite-element package, FIDAP. Natural convection effects on fluid flow and heat transfer were studied using a Fluent-based model[14]. Various lab studies exist for carbon combustion in mold powders[5,9]. In the work by Schwerdtferger[5], large samples were oxidized by keeping them at a constant temperature. In the real casting process, temperature gradients exist within the powder, and it is important to understand the combustion behavior in mold powders.

The current work introduces computational models of heat transfer, fluid flow, mass transfer, and thermodynamics (combustion reactions), which can predict how the powder slag layer thicknesses, temperature profile, and melting rate vary with time, and distance through the powder/slag layers. It considers the effect of powder densification due to sintering process, powder melting

© 2025 by the Association for Iron & Steel Technology.

to form liquid flux, the consumption of liquid flux (to lubricate the gap), power addition at the top surface to define the powder/slag layer thicknesses, carbon combustion under a thermal gradient, gas evolution, transport and off-gas release as exhaust from the top surface. The next section describes a transient thermal model, followed by the other submodels of a new Multi-physics model to describe these phenomena occurring in the mold powder layers.

COMPUTATIONAL MODEL DEVELOPMENT

Transient Thermal Model

The powder/slag region (Figure 2 (b)) is modeled from the top of the molten steel interface with the liquid slag, to the top of the powder layer and some of the air above (which takes away heat to the environment, and supplies oxygen). A one-dimensional (1-D), finite-difference-based fixed-grid model has been developed in MATLAB, to compute the heat and mass transfer during transients in the process. This domain represents a typical local region of the powder layer surface. However, for initial simulations, it is considered to represent an average powder/slag thickness to which an air layer is added, to handle the rises and drops in the powder level due to the combined actions of powder addition, powder shrinkage, and liquid flux consumption.

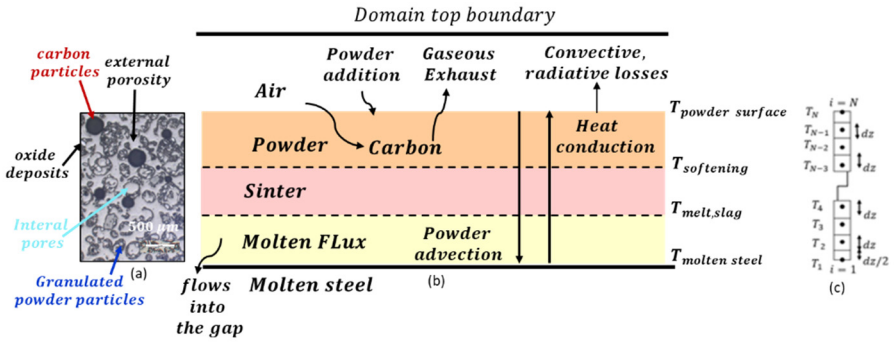

Figure 2: Closeup of powder / slag layers showing (a) Optical micrograph of mold powder structure[4] (b) Model domain (c) Corresponding grid of computational cells.

Liquid flux consumption can be quantified in several different ways, such as downward velocity through the various powder layers (mm/s), as shown in Figure 2 (b), consumption averaged over the external surface area (length and width directions) of the moving solidifying steel shell as it is withdrawn downwards at the casting speed (kg/m^2), addition rate of powder to the top surface according to the bags added per hour (kg/hr.), or, consumption of the liquid slag into the interfacial gap per oscillation cycle (g/m-cycle). These different measures are equivalent and each of them determines the rate of powder usage, based on the strand dimensions, casting speed, mold oscillation frequency, and local density. Higher casting speeds result in greater powder consumption.

Heat and mass flow are considered in the vertical direction, z, of the 1-D domain (Figure 2(b)) which represents the layers of liquid flux, powder/sinter, and some air. Heat supplied from the molten steel is conducted upwards through these various layers. Heat is also advected downwards due to the powder shrinkage and liquid flux removal from the bottom (liquid slag layer) due to consumption. Heat leaves the powder top surface (powder-air interface) due to convection and radiation. Thermal properties, including thermal conductivity, specific heat, and density, are temperature dependent, and increase towards the bottom of the domain.

Gas transport and combustion are modeled in the powder layers. Combustion consumes free carbon, as carbonate decomposition is not considered in the current model. A constant pressure of 1 atm is assumed in the entire domain, because the entire powder layer is thin, with very low density and high porosity, so has very high permeability. Thus, any pressure build-up is neglected in the model.

The macroscopic interfaces or phase boundaries between the air, powder/sinter and liquid flux layers evolve with time according to heat flow and mass transfer between the cells in the domain. The top of the top cell in the computational domain (as well as other cells in the region above the loose powder) is comprised of air and is set to an ambient temperature of 300K (domain top boundary). The bottom of the bottom cell at $z = 0$ in the domain represents the interface between the top surface of the molten steel and the bottom of the liquid slag layer (domain bottom boundary). This bottom boundary is fixed at the local temperature of the molten steel. The number and size of the cells in the domain are fixed. However, the phase of each cell can change with time due to the mass transfer associated with shrinkage of the powder column, powder addition at the top surface, and advection of powder down through the domain, according to the consumption.

© 2025 by the Association for Iron & Steel Technology.

The model equations for heat, mass transfer, and interfacial movement are as follows:

$$\rho c_p \frac{\partial T}{\partial t} = \rho c_p v_{cons,f} \frac{\partial T}{\partial z} + \rho c_p v_{shrink,p} \frac{\partial T}{\partial z} + k \frac{\partial^2 T}{\partial z^2} + \frac{\partial k}{\partial T}\left(\frac{\partial T}{\partial z}\right)^2 \quad (1)$$

$$\frac{dm_p}{dt} = \dot{m_{add,p}} - \dot{m_{cons,f}} - \dot{m_{advection}} \quad (2)$$

$$w_{inter(2,r+1)} = w_{final(2,r)} - \frac{\dot{m_{cons,f}} * dt_{sel}}{rho_f * A_c} \quad \text{(Liquid flux - sinter interface)} \quad (3)$$

$$w_{inter(3,r+1)} = w_{final(3,r)} - \frac{\dot{m_{cons,f}} * dt_{sel}}{rho_f * A_c} - ht_{shrinage} \quad \text{(Powder top surface)} \quad (4)$$

where: ρ: $density$ [kg/m^3], rho_f: liquid flux density [2600 kg/m^3], c_p: specific heat [J/kgK], T: temperature [K], t: time [s], dt_{sel}: time step size [s], $v_{cons,f}$: slag consumption velocity [m/s], $v_{shrink,p}$: powder shrinkage velocity [m/s], z: distance from the domain bottom [m], k: thermal conductivity [W/m-K], m_p: powder mass in cell [kg], $\dot{m_{add,p}}$: powder addition rate [kg/s], $\dot{m_{cons,f}}$: liquid flux consumption rate [kg/s], $\dot{m_{advection}}$: powder advection rate due to sintering [kg/s], r: previous time step [#], $r+1$: current time step [#], $w_{inter(2,r+1)}$: liquid-flux-sinter interface [m], $w_{final(2,r)}$: flux-sinter interface at previous time step [m], $w_{inter(3,r+1)}$: powder top surface [m], $w_{final(3,r)}$: powder top surface at previous time step [m], A_c: strand cross-section area [m^2], $ht_{shrinage}$: level drop in the powder/sinter layer due to powder shrinkage [m].

Equations (1) and (2) represent the energy and mass balance through mold powder/slag layers, and Equations (3) and (4) represent the powder/slag interfacial movement needed for mass balance. Any interface movement due to melting is calculated using linear interpolation of nodal temperatures and known phase melting temperatures.

A flowchart of the new computational models showing the constituent submodels is presented in Figure 3. The red and green boxes show the components of the transient thermal model explained above. The other boxes contain the other submodels which comprise the multiphysics model. As described in the following sections, these include a sintering submodel implemented in the thermal property subroutines, (of pore fraction, density, thermal conductivity), a gas transport submodel and a combustion submodel of carbon and gas reactions that have been developed to predict the carbon and gas distribution, based on previous models and measurements of lab sintering[9]. Next, the transient thermal model is verified with simulations using the Fluent commercial package. Then, the multiphysics model is applied and compared with a lab sintering experiment, where detailed measurements are available for model validation. This experiment did not involve a liquid flux layer. Finally, a simulation of powder behavior in the real steel continuous-casting process is presented.

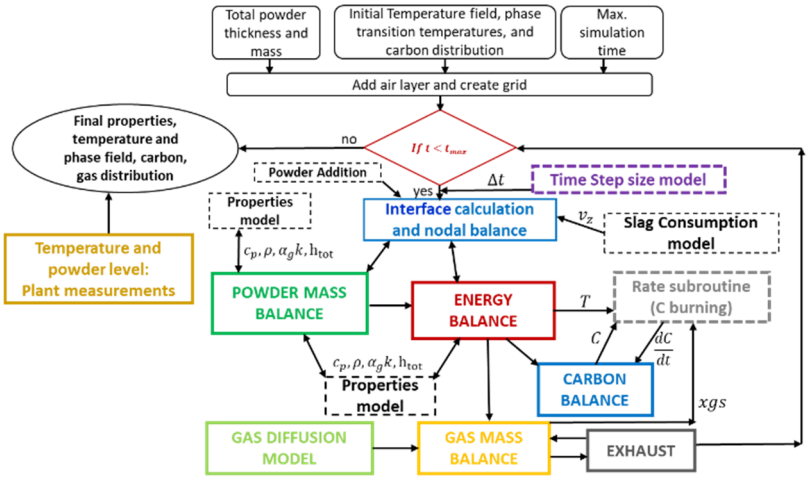

Figure 3: Model Flow chart showing calculation procedure.

Sintering Model

Granulated powders have a very high porosity (≥70%) at room temperature, because they contain both internal pores inside each relatively hollow particle and external pores between particles, as shown in *Figure 2* (a). As the powder heats up, these particles become more closely packed, and the total porosity decreases. Thus, the particle density increases with both higher

© 2025 by the Association for Iron & Steel Technology.

temperatures and longer times. Sintering rate kinetics to quantify this are given from previous literature as follows,[9,17,18] with parameters used in the current model provided in Table 1.

$$\frac{(\rho_{app-}\ \rho_{app}^{0})\rho_s}{(\rho_s\ -\rho_{app}\ )\rho_{app}^{0}} = K_s t^n \tag{5}$$

$$\alpha_g = 1 - \frac{\rho_{app}}{\rho_s} \tag{6}$$

$$k_{eff} = \left(\frac{1-\alpha_g^{\frac{1}{3}}}{k_{solid}} + \frac{\alpha_g^{\frac{1}{3}}}{\left(1-\alpha_g^{\frac{2}{3}}\right)k_{solid} + \alpha_g^{\frac{2}{3}} k_{gas}} \right)^{-1} \tag{7}$$

Table 1: Parameters used for densification calculation in current model.

Property/variable	**Unit/Value**
Apparent density, ρ_{app}^{0} (cold powder at 300K)	0.62 g/cm^3
Solid powder density, ρ_s (fully sintered)	2.7 g/cm^3
Instantaneous powder density, ρ_{app}	g/cm^3
Sintering rate constant, K_s (Based on experiments by Supradist et.al[9])	0 (T<400℃) 600℃ : 0.036 mass fraction min$^{-0.5}$ 800℃ : 0.045 mass fraction min$^{-0.5}$ 1000℃ : 0.361 mass fraction min$^{-0.5}$
Solid powder conductivity, k_{solid}	2 W/mK
Gas thermal conductivity, k_{gas}	0.026 W/mK
Effective thermal conductivity, k_{eff}	W/mK
Void/Pore fraction, α_g	#
Time, t	min
Parameter, n	0.5

Combustion model of Carbon and Gas Balances Combustion in the mold powder at a given time, t, during a simulation depends on the remaining carbon content, temperature, and gas content at the given location in the powder layers. Various phenomena need to be considered to accurately predict the carbon and gas distribution through the mold powders, including the chemical reaction kinetics, gas diffusion and transport through the pores, and gas exhaust from the top surface to ambient. These in turn depend on the temperature and phase compositions calculated by the thermal and sintering models described in the previous section. Depending on the temperature and pore distribution through powder, the combustion physics in certain regions of the powder can be reaction-controlled, or diffusion-controlled. The temperature and properties calculated by the heat and mass transfer model along with the sintering model results are input to this carbon and gas balance model. Gas diffusion also depends on two factors: (i) Kinetic effect- due to the thermal effects and (ii) Tortuosity effect- due to pore size, distribution, and powder particle size distribution. As the powder heats up, the carbon and gas distributions evolve to reach near-equilibrium at long times.

A multi-species, 4-equation combustion model (4-eCM) has been used to calculate the chemical reaction rates, and obtain the resulting carbon and gas distributions. The rates of combustion reactions (mol/cm^{3}min) are available in literature.[5,9,19,20.]

© 2025 by the Association for Iron & Steel Technology.

r_1: $C + O_2 = CO_2$ (8)

r_2: $C + CO_2 = 2CO$ (9)

r_3: $CO + O_2 = CO_2 + O$ (10)

r_4: $CO + O + M^+ = CO_2 + M^+$ (11)

SIMULATION DETAILS

The computational domain is discretized into a fixed, uniformly-spaced grid that initially contains only air and powder layers. The powder thickness generally varies from 35-55 mm thickness. A grid size of 0.1mm is used in this work, based on previous verification simulations using a Steady State Model[21] which showed grid-independence with this spacing. The Steady-State Model itself was verified with ANSYS Fluent and analytical equations for constant properties. An explicit discretization scheme was used for the model to calculate the temperature, carbon, and gas distribution. Time-step size criteria based on heat conduction, advection, and gas diffusion were implemented for solution stability of this explicit model[22].

As the powder thermal diffusivity, shrinkage velocity, and gas diffusivity vary throughout the domain with time, the cell with the maximum value of these properties and criteria limits the time step size. The time-step size criteria are based on powder shrinkage velocity, flux consumption velocity, powder thermal and gas diffusivity. They are checked at every time step to make sure all the stability criteria are satisfied. The time-step size for heat transfer simulations was typically ~ $1.6*10^{-3}$ s. But while solving the combustion and gas reactions, due to high gas diffusivity through the porous powder bed, the time step size became about 100 times smaller (~$1.6*10^{-5}$ s). This explicit model took 5 days to run two hours of combustion and gas transfer calculations on a single node workstation (AMD Ryzen Threadripper PRO 5995WX, 2.7 Ghz, 512GB RAM).

RESULTS AND DISCUSSION

This section contains model results for: 1) verification of the transient thermal model with previous models of the top-surface powder/sinter and liquid flux layers in a continuous caster; 2) validation of the complete model system (multiphysics model) with measurements and previous model results for a lab sintering and combustion experiment[9] and 3) application and further validation of the transient thermal model with previous plant measurements at a continuous caster at Dofasco[15].

Thermal Model Verification Simulation

First, to verify the heat transfer model, transient heating of powder in a steel continuous caster was simulated with two different computational models. Conditions were chosen to match a particular trial with HSLA steel in the Dofasco plant.[15] First, a simulation was conducted using the commercial code, Fluent, with the axisymmetric domain shown in Figure 4(a).[15] Temperature-dependent thermal properties are shown in Figure 4(b). [15] A constant powder/slag density of 2600 kg/m^3 was used. Other parameters are given in Table 2, including a liquid flux consumption rate of 60.1 kg/hr. Starting with a steady-state solution for 40 mm of cold powder, 10 mm of cold powder was added to the top surface, and thicknesses were assumed to remain constant while calculating transient evolution of the thermal profile.

Table 2: Casting conditions for the trial considered for model verification.

Casting conditions/Parameters	Value
Casting speed	1.4 m/min
Axial advection velocity	2.43e-5 m/s
Molten Steel temperature	1823 K
Liquid flux- Sinter phase transition temperature	1400 K
Sinter- Powder phase transition temperature	1300 K
Strand width	1207 mm
Strand thickness	220 mm
Slag density	2600 kg/m^3
Heat transfer coefficient	3.3 W/m^2 K

© 2025 by the Association for Iron & Steel Technology.

Next, the current MATLAB-based transient thermal model was run for similar conditions to compare the thermal profiles at different times. A time-step size of 0.0023s was used. The temperature at the powder top surface for the 40mm slag layer was measured from pyrometer readings at the plant to be 705 K (432°C). This roughly matches the initial temperature at 40mm in both the Fluent and Matlab simulations. After 1 hour of simulation, temperature is still far below the steady-state distribution, which is never reached in practical plant operations.

The Matlab model results shown in Figure 4 (d) agree well with the Fluent model results shown in Figure 4(c). This verifies the current heat transfer model, which is next applied to a lab sintering experiment and to a continuous caster where more comprehensive measurements were available.

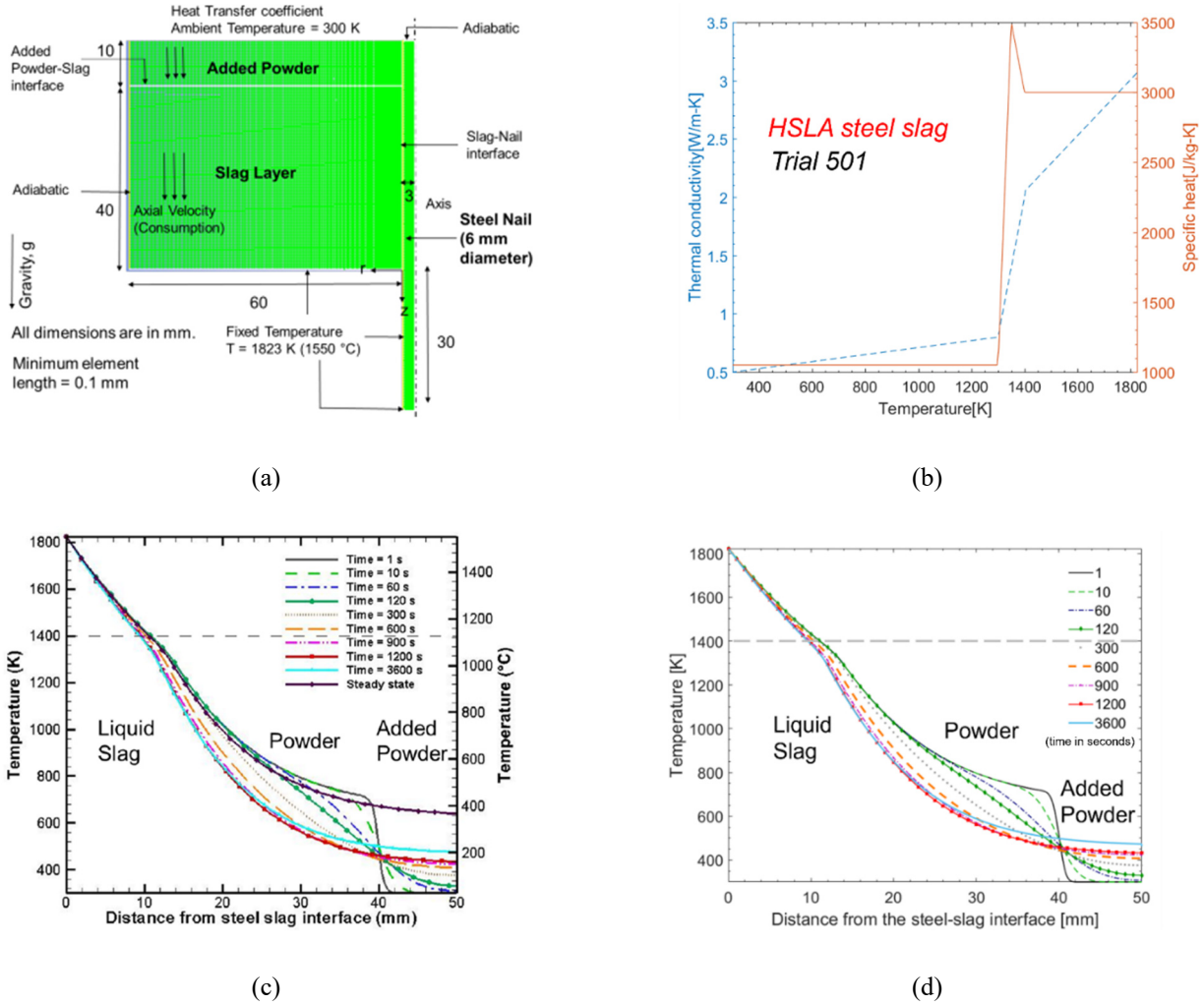

Figure 4: Transient Model verification (a) Mesh for the Fluent model[15] (b) Thermal properties (c) Fluent model thermal profile[15] (d) MATLAB model.

Lab Experiment Simulation

Next, the model system, including the thermal and mass balance model and the kinetics model, was applied to predict the temperature distribution, powder shrinkage due to densification, and pore fraction evolution for the lab experiment of powder sintering[9] shown in Figure 5. This simulation was simplified, relative to the continuous-casting environment in the plant, because the temperature was too low to form a liquid flux layer, and there was no slag consumption. The powder shrinkage prediction was validated with measurements, and the temperature predictions were verified with a previous model, which had itself been validated with this same experiment.[9] The current model was further extended to simulate multi-species combustion reactions, gas diffusion through the powder, and exhaust gas evolution, to predict the carbon and gas distributions through the powder/sinter layer. The effects of shrinkage velocity on the resulting temperature, carbon, and gas distributions due to downward mass transfer are currently neglected.

© 2025 by the Association for Iron & Steel Technology.

In the lab sintering experiment, cold powder (premixed with 5 wt.% graphite) was placed in a quartz tube and heated in a furnace for two hours[9]. The off-gas was collected by first passing it through a filter, then a flow analyzer, and finally into a gas hood. The setup is shown in Figure 5 (a).

The current model was run to obtain the temperature distribution in the powder. The density profile and thermal properties used in this run are shown in Figure 6. The transition temperatures where the sintering rate continuously changes slope are reflected in the thermal conductivity profile shown in Figure 6(b). Specifically, as temperature increases, the powder particles sinter to become more densely packed, and the pore fraction decreases, so the effective conductivity of the powder increases.

The predicted thermal profiles and temperature contours are shown in

Figure 7. Starting from ambient temperature (300K), the powder gradually heats from the bottom up. The powder bottom reaches the furnace temperature almost instantaneously, while the interior heats more slowly. Temperature decreases towards the top surface. Due to sintering, the powder undergoes densification, so the total thickness drops with time. This can be seen clearly in Figure 7(a) where the top point in each temperature profile is lower at each time (min).

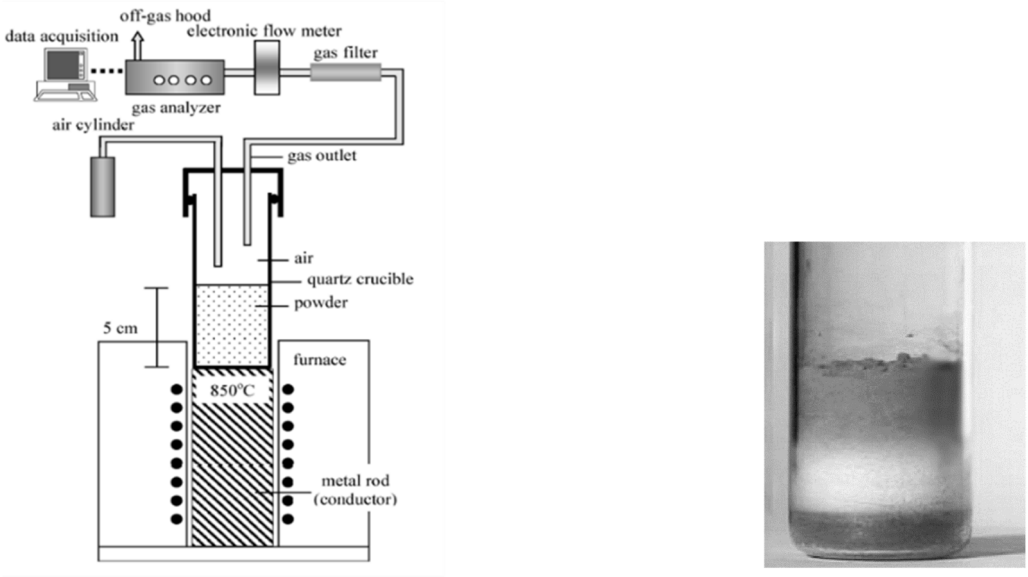

(a) (b)

Figure 5: (a) Lab setup for powder sintering and combustion experiments[9] (b) Quartz tube (on top of the furnace in the left figure) containing mold powder after experiment, showing carbon content (darkened)[9].

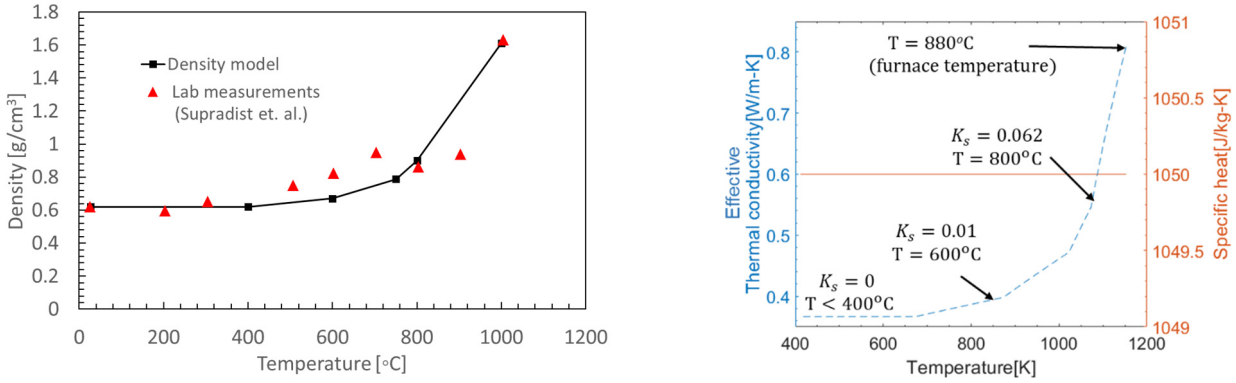

(a) (b)

Figure 6: (a) Density profile used in the current model (b) Thermal properties, and sintering rate constant (K_s).

© 2025 by the Association for Iron & Steel Technology.

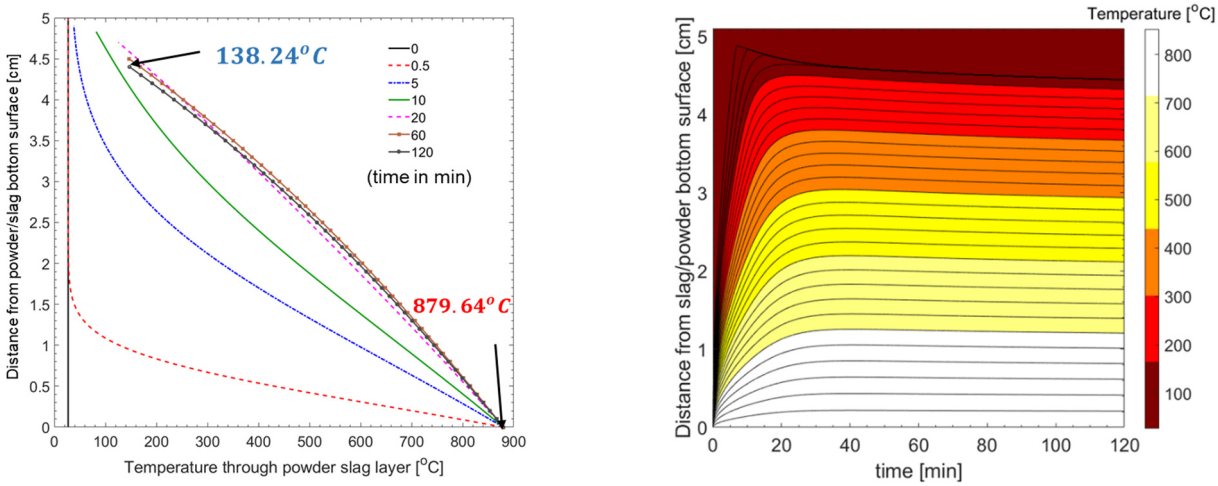

(a) (b)

Figure 7: (a) Temperature profile in the powder (b) Thermal contours.

The net powder shrinkage is compared with measurements[9] and with previous model calculations[9] in Figure 8(a). The current Matlab model predicts slightly more shrinkage compared to measurements but the agreement is reasonable. The evolution of pore fraction is shown in Figure 8 (b).

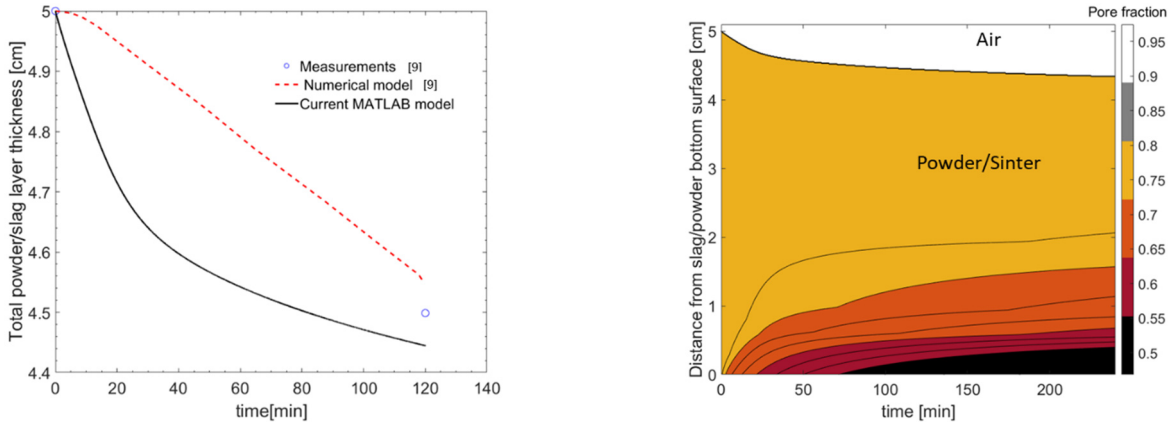

(a) (b)

Figure 8: Evolution of (a) Powder shrinkage validation (b) Pore fraction distribution

An example of the multiphysics model predictions during the time evolution of the reaction rates, carbon distribution and different gas species of the lab sintering experiment is given in Figure *9*. Initially, cold powder at room temperature has a uniform carbon content (volume fraction of 0.0141). Initially, the reaction rates are zero in the cold powder. As the temperature gradient develops in the powder, combustion causes the carbon distribution to become non-uniform. Towards the top of the cold powder, the temperature is too low for any reactions, so the carbon content stays at its initial constant value. Towards the middle of the powder, carbon combustion occurs by reaction with oxygen in the pores in and between powder particles to form carbon dioxide. Carbon dioxide is also produced by decomposition of CO rising up from lower in the powder. This consumes oxygen according to the molar balance of the reactions involving carbon dioxide (r_1 and r_3). The gas products expand according to the local increasing temperature, and cannot be accommodated in the available pore space. Thus, they rise to the top surface and exit the domain as exhaust. This decreases oxygen content inside the domain to negligible mole fractions (~10^{-26}).

Deeper into the powder, even though the temperature is higher, there is negligible oxygen, so carbon combustion cannot occur (small r_3). Thus, carbon content again stays closer to its initial value. Even deeper, near the bottom of the container, even higher temperature enables the endothermic Boudouard reaction should consume some carbon into producing carbon monoxide from some CO2 that diffuses downward from the pores above. However, diffusion was not included in this simulation, so the rate

© 2025 by the Association for Iron & Steel Technology.

of this reaction (r_2) is small until very near the bottom of the container. As seen in the gas distribution plots, the carbon dioxide content decreases towards the bottom, as the carbon monoxide content increases. Atomic oxygen has the lowest concentration among all the gases and is found to be highest in the powder mid-zone. Nitrogen is an inert gas not participating in any of these chemical reactions, so its concentration drops due to exhaust alone. The important effect of nitrogen is to take up space in the pores and to change the concentration of the oxygen and combustion gases.

The multiphysics model predictions of carbon distribution (Figure 10 (a)) are compared with measurements of the lab sintering experiment[9] in Figure 10 (b) . Reasonable qualitative agreement is observed. There is very little combustion towards the top of the powder. Midway down the powder column, carbon is consumed by combustion, where a minimum is observed. Towards the bottom, carbon accumulation is observed in the measurements. The higher carbon in this region is also seen in the model curve, but the increase above the initial carbon content is not predicted, so the model curve is lower. This is because the downward movement of carbon due to shrinkage is not yet considered in the model. Including this effect is expected to shift the predicted curve downwards and to enable some accumulation, resulting in even better agreement with the measurements[23]. In the continuous caster, this accumulation is enhanced by consumption and results in a significantly C-enriched sinter layer, which has been widely reported in the powder layers of operating steel continuous casters[2].

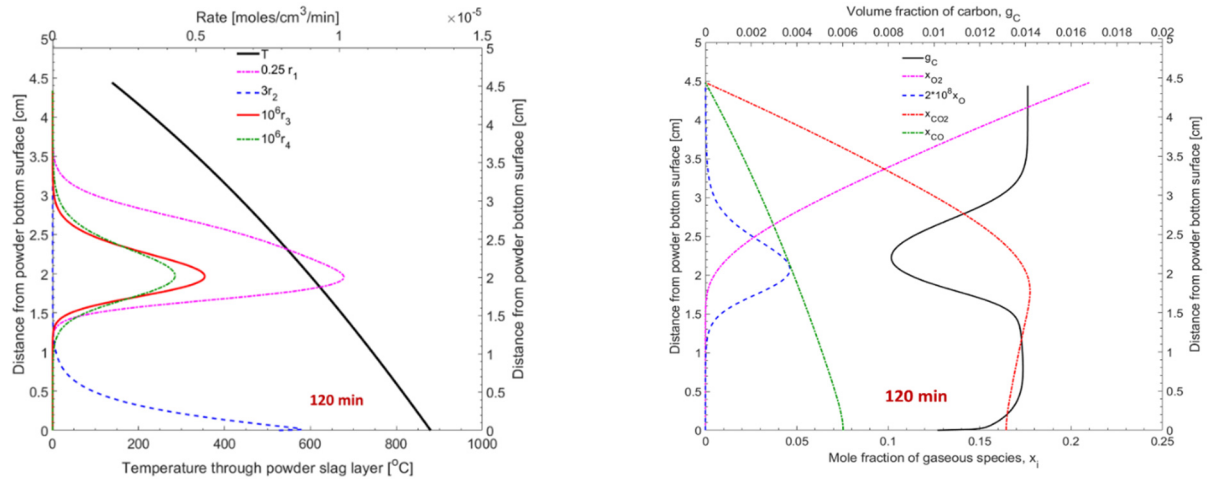

(a) (b)

Figure 9 Model predictions at 120 min (a) Temperature (T) and reaction rates (r_1, r_2, r_3, r_4) (b) Carbon volume fraction (g_C), and mole fractions of oxygen, carbon dioxide, and carbon monoxide ($x_{O_2}, x_O, x_{CO_2}, x_{CO}$).

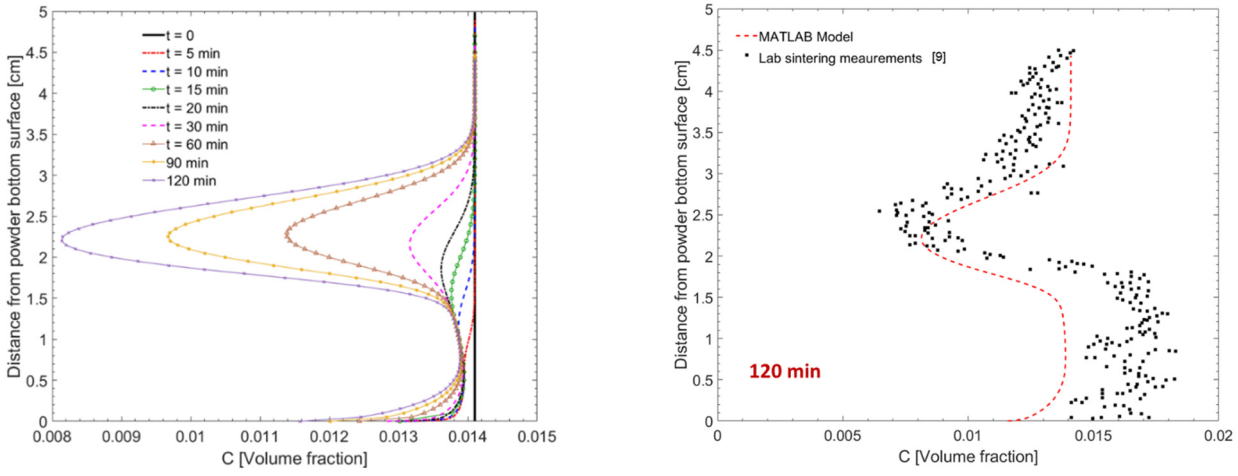

(a) (b)

Figure 10: Carbon profile (a) Transient evolution (b) Model validation with lab sintering experiments.

© 2025 by the Association for Iron & Steel Technology.

Continuous Caster Simulation

Finally, the transient thermal model has been applied to simulate heat and mass-transfer behavior in the powder layers in several commercial steel continuous casters, where plant measurements of the evolution of temperature and powder thickness were available. An example of the casting conditions for one of these simulations is given in Table 3. The initial powder thickness of 39.2 mm was based on averaging the measurement data, and the initial temperature distribution is calculated using the in-house Steady-State Model. A time frame including five powder addition cycles was simulated to enable reasonable validation.

Preliminary results of powder level and temperature are shown in Figure 11, which neglect the effects of powder shrinkage due to sintering, combustion, and gas transport. Lines were drawn through the measured data points according to estimates of the powder addition times, and the measured heights after powder addition and corresponding addition times were input to the model. Both the predictions and measurements in Figure 11(a) show how the powder level goes up and down during the casting process. As the casting process starts, liquid flux is consumed according to the axial advection velocity based on powder consumption into the gap between the solidifying shell and the water-cooled copper mold. This causes a gradual drop in the powder levels. Lower powder levels enhance heat conduction, which in turn increases powder melting, so the liquid flux layer thickness increases. At this plant, manual powder addition occurred whenever the operator noticed red spots, indicating zones of high temperature, at the powder top surface. There is no quantitative determination of how much powder should be added at what times. The lack of this quantitative knowledge is one of the underlying motivations for building this model. Most plants operate with a "black" practice, meaning that powder is added to maintain surface temperatures below the visible threshold.

After each powder addition, the surface temperature suddenly drops to ambient (300K), due to the cold powder. Then, as casting continues, the powder gradually heats up, and the liquid slag layer keeps building. Figure 11(a) shows that the measured powder consumption input to the model is consistent with the observed drop in powder level between powder additions. Figure 11(b) shows that a reasonable match is obtained between the model predictions and plant measurements of powder top-surface temperature. Finally, the model predicts gradual buildup of the liquid flux layer over long time periods, although this has not yet been checked by plant measurements.

Table 3: Casting conditions for ultra-low carbon steel slag in continuous caster

Casting conditions/Parameters	Value
Casting speed	1.2 m/min
Axial advection velocity (flux consumption)	2.3×10^{-5} m/s
Molten Steel temperature	1823 K
Liquid flux- Sinter phase transition temperature	1398 K
Sinter- Powder phase transition temperature	1368 K
Strand width	1531 mm
Strand thickness	220 mm
Powder/slag density	2600 kg/m^3
Average powder slag thickness	39.2mm

© 2025 by the Association for Iron & Steel Technology.

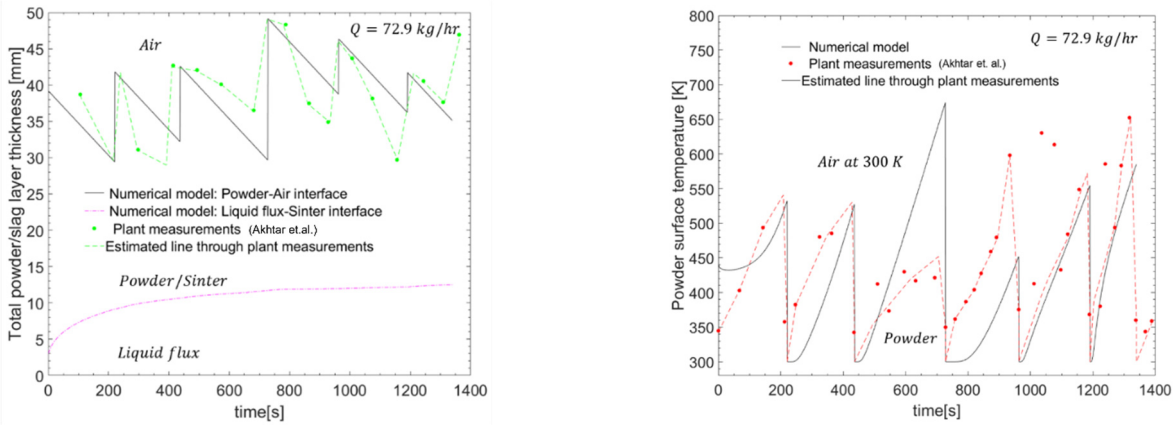

(a) (b)

Figure 11: Model validation comparing predicted and measured (a) Powder/slag level (b) Powder surface temperature

CONCLUSIONS

A multi-physics model has been developed to estimate the transient temperature distribution, sintering kinetics, phase-change behavior, mass transport, carbon combustion, and gas transport through the top-surface powder/sinter and liquid flux layers during continuous casting of steel. The model evaluates rate kinetics equations to calculate the powder properties and pore fraction in the powder/slag column and considers the effect of sintering. Powder densification due to sintering decreases the pore fraction which causes shrinkage and an increase in the thermal conductivity, density, and temperature. The model also can predict the carbon and gas distributions due to chemical reactions involving carbon burning. The equations are solved using an explicit, one-dimensional finite-difference model in Matlab. The transient thermal model has been verified with a 2D simulation using Fluent and with steel continuous casters. The multiphysics model is validated with temperature measurements in a lab-sintering experiment[9]. Measurements in the lab experiments are also used to validate the model predictions of sintering kinetics and carbon distribution.

It is found that considering the density variation through the powder/slag layers (initial phase-dependent density for the caster, or accurate density estimate by implementing sintering kinetics) is important to accurately predict the level changes in the powder, and therefore the resulting temperature distribution. In a caster, powder surface temperature drops to ambient during powder additions, and heats up in between, which results in powder melting to form liquid flux. The temperatures in a caster never reach steady-state for practical purposes as transients prevail in the plant due to intermittent powder additions occurring every 3-5 minutes. The carbon distribution trend through the powder slag layer captures the various multiphysics phenomena occurring due to heat and mass transfer, densification, and chemical reactions.

ACKNOWLEDGEMENTS

The authors would like to thank personnel at Dofasco, Canada (including Joydeep Sengupta and Bruce Farand), Matthew Zappulla, and TATA Steel, Netherlands, for providing measurements for model validation. This work is supported by the Continuous Casting Center at the Colorado School of Mines, Golden, CO.

REFERENCES

1. Y. Meng and B. G. Thomas, “Simulation of Microstructure and Behavior of Interfacial Mold Slag Layers in Continuous Casting of Steel,” *ISIJ international*, vol. 46, no. 5, pp. 660–669, 2006, doi: 10.2355/isijinternational.46.660
2. T. Nakano, M. Fuji, K. Nagano, T. Matsuyama, and N. Masuo, “Model analysis of melting process of mold powder for continuous casting of steel”, *Nippon steel technical report. Overseas*, vol. 34, pp.21-30, 1987.
3. Kenneth C. Mills, Carl-Åke Däcker, “Manufacture of Mould Fluxes”, *The Casting Powders Book*, Springer, 2018, pp. 279-280. https://doi.org/10.1007/978-3-319-53616-3
4. Jan Kromhout, TATA Steel, “Standard mould powder for thin slab casting (DSP)”, *Plant Report*, IJmuiden, Netherlands, 2023

© 2025 by the Association for Iron & Steel Technology.

5. K. Schwerdtfeger and A. Jablonka, “Kinetics of carbon combustion in packings of casting powder,” *Steel research*, vol. 64, no. 1, pp. 77–86, 1993, doi: 10.1002/srin.199300986.

6. A. Akhtar, B. G. Thomas, J. Sengupta, “Analysis of Nail Board Measurement of Liquid Slag Layer Depth,” *AISTech 2016 −Proceedings of the Iron and Steel Technology Conference*, pp. 1427–1438.

7. H. Nakato, T. Sakuraya, T. Nozaki, T. Emi, and H. Nishikawa, “Physical and chemical properties of casting powders affecting the mold lubrication during continuous casting,” *Steelmaking Proceedings*, vol. 69, pp. 137-143,1986.

8. A. Delhalle, M. Larrecq, J. Marioton, and P. Riboud, “Slag melting and behaviour at meniscus level in a CC mold,” *Steelmaking Proceedings* , vol. 69, pp. 145-152,1986.

9. M. Supradist, A. W. Cramb, K. Schwerdtfeger, “Combustion of Carbon in Casting Powder in a Temperature Gradient,” *ISIJ International*, vol. 44, no. 5, pp. 817-826, 2004, doi: 10.2355/isijinternational.44.817.

10. K. Spitzer, J. Holzhauser, F. Bruckner, B. Siera, H. Grethe, K. Schwerdtfeger, “New measuring methods for the assessment of flux powders,” *Stahl und Eisen*, vol. 108, no. 9, pp. 441-450, 1988.

11. M. Kawamoto, T. Watanabe, T. Ikeda, “Melting behavior of mold powder for continuous casting of steel by thermo mechanical analysis,” *Tetsu-to-hagan´e,* vol. 81, no. 12, pp. 1132-1137, 1995.

12. K. Mills, A. Olusanya, R. Brooks, R. Morrell, S. Bagha, “Physical properties of casting powders. IV. physical properties relevant to fluid and thermal flow*,” Ironmaking Steelmaking,* vol 15, no. 5, pp. 257-264, 1988.

13. R. McDavid, “Flow and thermal behavior of the top surface flux/powders in continuous casting molds,” M.S. Thesis, University of Illinois, Urbana Champaign, 1994.

14. B. Zhao, S. Vanka, and B. Thomas, “Numerical study of flow and heat transfer in a molten flux layer,” *International journal of heat and fluid flow*, vol. 26, no. 1, pp. 105–118, 2005, doi: 10.1016/j.ijheatfluidflow.2004.05.016.

15. A. Akhtar, “Analysis of the nail board experiment to measure the liquid slag depth in steel continuous casting”, M.S. Thesis, University of Illinois, Urbana-Champaign, 2016.

16. A. Jonayat, B. G. Thomas, “Transient thermo-fluid model of meniscus behavior and slag consumption in steel continuous casting,” *Metallurgical and Materials Transactions B* , vol. 45, pp. 1842-1864, 2014.

17. F. Th¨ummler, W. Thomma, “The sintering process,” *Metallurgical Reviews*, vol. 12, no. 1, pp. 69-108, 1967.

18. J. Rekola, “Isothermal sintering kinetics of uosub (2+ x),”, Ph.D. Thesis, Helsinki Univ. of Technology, 1978.

19. E. Turkdogan, J. Vinters, “Effect of carbon monoxide on the rate of oxidation of charcoal, graphite and coke in carbon dioxide,” *Carbon*, vol. 8, no. 1, pp. 39-53, 1970, https://doi.org/10.1016/0008-6223(70)90127-2.

20. J. Warnatz, U. Maas, R. W. Dibble, *Combustion*, “Chemical Kinetics”, Springer, 2006.

21. L.Das, Colorado School of Mines, *Continuous Casting Center 2019 report*, Golden, Colorado, 2019.

22. A. Hindmarsh, P. Gresho, D. Griffiths, “The Stability of Explicit Euler Time-Integration for Certain Finite Difference Approximations of the Multi-Dimensional Advection-Diffusion Equation”, *International Journal for Numerical Methods in Fluids*, vol. 4., pp.853 - 897. 1984, doi: 10.1002/fld.1650040905.

23. L. Das, “Modeling of Continuous Casting Mold Powder Behavior: Heat Transfer, Combustion, Sintering, and Melting”, Ph.D. Thesis, Colorado School of Mines, 2024.

© 2025 by the Association for Iron & Steel Technology.